

# Quantized Proximal Averaging Network for Analysis Sparse Coding

Kartheek Kumar Reddy Nareddy\*<sup>1</sup> Mani Madhoolika Bulusu\*<sup>1</sup> Praveen Kumar Pokala<sup>1</sup>  
Chandra Sekhar Seelamantula<sup>1</sup>

## Abstract

We solve the analysis sparse coding problem considering a combination of convex and non-convex sparsity promoting penalties. The multi-penalty formulation results in an iterative algorithm involving *proximal-averaging*. We then unfold the iterative algorithm into a trainable network that facilitates learning the sparsity prior. We also consider quantization of the network weights. Quantization makes neural networks efficient both in terms of memory and computation during inference, and also renders them compatible for low-precision hardware deployment. Our learning algorithm is based on a variant of the ADAM optimizer in which the quantizer is part of the forward pass and the gradients of the loss function are evaluated corresponding to the quantized weights while doing a book-keeping of the high-precision weights. We demonstrate applications to compressed image recovery and magnetic resonance image reconstruction. The proposed approach offers superior reconstruction accuracy and quality than state-of-the-art unfolding techniques and the performance degradation is minimal even when the weights are subjected to extreme quantization.

**Keywords:** Analysis sparse model, Quantized neural networks, Compressed sensing, Compressed image recovery, Proximal averaging.

## 1. Introduction

The objective in Compressive Sensing (CS) is to reconstruct a sparse signal  $\mathbf{x} \in \mathbb{R}^n$  from its compressed observation,  $\mathbf{y} = \Phi\mathbf{x} \in \mathbb{R}^m$ , where  $\Phi$  is an  $m \times n$  matrix, with  $m \ll n$ . The standard convex optimization formulation to solve the

\*Equal contribution <sup>1</sup>Electrical Engineering, Indian Institute of Science. Correspondence to: Kartheek Kumar Reddy Nareddy <nareddyreddy@iisc.ac.in>.

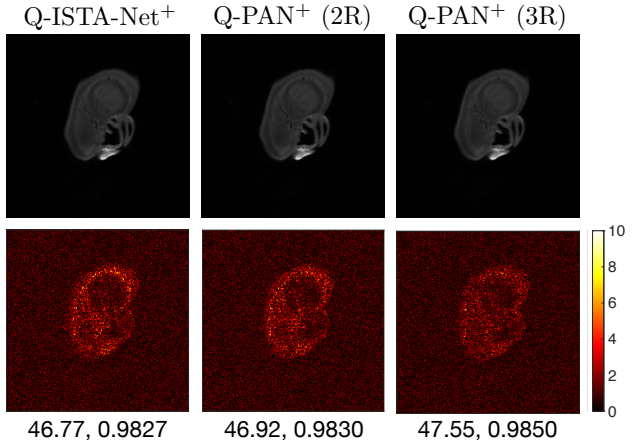


Figure 1: Brain MRI image reconstruction for CS ratio 40% by the proposed 1-bit Quantized models. The bottom row visualizes the absolute difference between the ground truth and the reconstructed images. The Q-PAN<sup>+</sup> (3R) model captured the brain structure better and hence the difference image is majorly composed of noise. The numbers indicate the PSNR, SSIM values.

CS problem is given as follows:

$$\min_{\mathbf{x}} \frac{1}{2} \|\Phi\mathbf{x} - \mathbf{y}\|_2^2 + \lambda \|\Psi\mathbf{x}\|_1, \quad (1)$$

where  $\mathbf{y}$  is the observation,  $\Psi$  is the sparsifying transform for  $\mathbf{x}$ , and sparsity is enforced on  $\Psi\mathbf{x}$  using an appropriate regularizer, which in this case is the  $\ell_1$ -norm, and  $\lambda$  is the regularization parameter.

However it has been shown that  $\ell_1$ -norm regularization results in biased amplitude estimates (Zhang, 2010). Non-convex regularizers are known to reduce the bias in the estimates. One can design efficient non-convex regularizers by considering a combination of several sparsity-promoting regularizers.

The CS framework has enabled several practical applications particularly in the context of computational imaging (Willett et al., 2012), ultrasound imaging (Quinsac et al., 2010), magnetic resonance imaging (Jacob et al., 2020), cognitive radar (Stinco et al., 2014), cognitive radio (Tian & Giannakis, 2007), etc.

Sparse recovery algorithms are iterative and involve manual parameter tuning and several iterations to achieve accurate reconstruction. Iterative algorithms when unfolded into a feedforward neural network architecture can greatly enhance the reconstruction accuracy since the network has the advantage of *learnability*. Further, the depth of the network is also significantly lower than the number of iterations of the algorithm from which it is inspired. Therefore, the inference time is reduced. However, the price to pay for these advantages is the overhead of training. A practical bottleneck in deploying such models is that they require more memory to store the high-precision weights and consequently also more computation. In applications involving low-precision hardware, the reconstruction accuracy reduces drastically. One of the issues that is addressed in this paper is the effect of weight quantization on the performance of unfolded networks. The objective is to obtain comparable accuracy to the full-precision scenario considering weights that are coarsely quantized (which we show in the Figure 1). Such *quantized unfolded networks* are more amenable to practical implementation particularly in resource constrained settings.

Another important aspect that we focus on in this paper is the problem of *analysis prior learning* using a combination of convex/non-convex sparsity promoting regularizers. The analysis prior is more effective than the synthesis prior because most naturally occurring signals and images are sparse only when analyzed using a suitable transformation (Rubinstein et al., 2013). Further, employing a combination of penalty functions has been shown to result in superior reconstruction performance than a single penalty function (Kamilov, 2017) and gives rise to the notion of *proximal averaging*. The penalty functions could be convex or non-convex. *Learning* a convex combination of penalty functions is also likely to improve the sparse recovery performance. Before proceeding with further developments, we review recent state of the art in these domains.

## 2. Prior Art

We present the literature in two categories, namely, quantized networks and analysis sparse recovery techniques.

*Quantized Networks* Neural Networks that employ binary weights and activations, also known as binary neural networks (BNNs) (Courbariaux et al., 2015; Hubara et al., 2016; 2018) have been shown to be promising for solving classification problems. Their efficacy has been demonstrated on MNIST (LeCun & Cortes, 2010) and CIFAR10 (Krizhevsky et al.) datasets. The XNOR-Net (Rastegari et al., 2016) used a gain term computed from the statistics of the weights to scale the binary weights in order to reduce the quantization error. The XNOR-Net performed relatively better than previous BNN architectures on the ImageNet (Deng

et al., 2009) dataset. The learned quantization networks (LQ-Net) (Zhang et al., 2018) was proposed to minimize the quantization error by jointly learning the quantizer and the network. The Bi-Real Network (Liu et al., 2018) employs residual connections where full-precision activations from the previous layer affect the quantization in the current layer. On the optimization front Meng et al. (2020) justified the straight-through-estimator (STE) method used for training the BNNs through bayesian learning. The quantization of weights has also been shown to be promising in the context of generative adversarial networks (GANs) (Wan et al., 2020; Wang et al., 2019). Zhu et al. (2020) adapts Neural Architecture Search (NAS) to find an optimized architecture for the binarization of Convolutional Neural Networks (CNNs). Duncan et al. (2020) showed that quantized neural networks are generally robust relative to their full precision counterpart against adversarial perturbations. While the role of quantization has been considered in classification and generation problems, it has been relatively unexplored in the context of optimizing unfolded networks for sparse recovery.

*Analysis Sparse Priors* Several works (Beck & Teboulle, 2009; Donoho et al., 2009; Elad et al., 2007; Liu et al., 2016) have considered the  $\ell_1$ -regularized analysis/synthesis sparse recovery problems owing to its convexity. In order to solve the CS problem in the context of recovering natural images, optimization based techniques assumed that the input images are sparse in a fixed transform domain such as the discrete cosine transform (DCT), wavelet domain (Sungkwang Mun & Fowler, 2009), gradient-domain (Li et al., 2013), etc. Denoising based AMP (D-AMP) (Metzler et al., 2016), etc. ensures good recovery for natural images. Most methods exploit structured sparsity of the data as an image prior and solve the problem iteratively (Kim et al., 2010; Li et al., 2013; Metzler et al., 2016; Zhang et al., 2014). All iterative sparse recovery methods require hundreds of iterations to solve Eq. (1), which inevitably gives rise to high computational overhead thus restricting the application of CS. In addition, the analysis operator or the hyperparameters such as learning rate and regularization parameter are usually hand-crafted.

To overcome the limitations of optimization based techniques, network-based approaches have been proposed recently. ReconNet is a neural network approach proposed in (Kulkarni et al., 2016), which takes in CS measurements of an image as input and outputs an intermediate reconstruction. Networks such as ISTA-Net (Zhang & Ghanem, 2018) performed better when the sparsifying transform was learned by imposing the  $\ell_1$  penalty on the prior. Two aspects are missing from current literature. First, finer approximation of  $\ell_0$  pseudonorm in the context of data-driven analysis-prior learning and second, reducing the model size and improved hardware-compatibility of the CS networks. We aim to

Table 1: Sparsity-promoting regularizers and corresponding proximal operators employed in this study.

NAME	PENALTY FUNCTION	PROXIMAL OPERATOR
$\ell_1$ - norm ( $\lambda > 0$ )	$g_1(x) = \lambda  x $	$\mathcal{P}_1(x) = \text{sgn}(x) \max( x  - \lambda, 0)$
MCP (ZHANG, 2010) ( $\lambda > 0, \gamma > 1$ )	$g_2(x) = \begin{cases} \lambda  x  - \frac{ x ^2}{2\lambda\gamma}, & \text{for }  x  \leq \gamma\lambda, \\ \frac{\lambda^2\gamma}{2}, & \text{for }  x  \geq \gamma\lambda. \end{cases}$	$\mathcal{P}_2(x) = \begin{cases} 0, & \text{for }  x  \leq \lambda, \\ \text{sgn}(x) \frac{\gamma}{\gamma-1} ( x  - \lambda), & \text{for } \lambda <  x  \leq \gamma\lambda, \\ x, & \text{for }  x  > \gamma\lambda. \end{cases}$
SCAD (FAN & LI, 2001) ( $\lambda > 0, a > 2$ )	$g_3(x) = \begin{cases} \lambda  x , & \text{for }  x  \leq \lambda, \\ \frac{ x ^2 - 2a\lambda x  + \lambda^2}{2(1-a)}, & \text{for } \lambda <  x  \leq a\lambda, \\ \frac{(a+1)\lambda^2}{2}, & \text{for }  x  > a\lambda. \end{cases}$	$\mathcal{P}_3(x) = \begin{cases} \text{sgn}(x) \max( x  - \lambda, 0), & \text{for }  x  \leq 2\lambda, \\ \frac{(a-1)x - \text{sgn}(x)a\lambda}{a-2}, & \text{for } 2\lambda <  x  \leq a\lambda, \\ x, & \text{for }  x  > a\lambda. \end{cases}$

address these two aspects with application to compressed image reconstruction.

### 3. Contribution of this Paper

Our contribution lies at the intersection between the two aspects – network quantization and optimization for analysis sparse prior learning while employing several regularizers. The starting point for the developments is a multi-penalty/composite regularization formulation of the sparse recovery problem in an analysis-sparse setting. The result is the proximal-averaged iterative shrinkage algorithm (PAISA), which when unfolded gives rise to the proximal-averaging network (PAN). It is in the context of PAN that we consider the effect of quantization (Q-PAN). On the application front, we consider image recovery from compressed measurements both for natural images and magnetic resonance images.

### 4. Composite Regularization in the Analysis Setting

Consider the problem of compressed sensing recovery based on multiple penalties  $\{g_i\}$  as given below:

$$\min_{\mathbf{x}} \frac{1}{2} \|\Phi \mathbf{x} - \mathbf{y}\|_2^2 + \underbrace{\sum_{i=1}^p \alpha_i g_i(\mathcal{F}(\mathbf{x}))}_{g(\mathbf{x})}$$

subject to  $\sum_{i=1}^p \alpha_i = 1, \quad 0 < \alpha_i < 1, \forall i, \quad (2)$

where  $\mathcal{F}$  is the data-driven, sparsifying, analysis operator and  $p$  is the number of sparsity-promoting regularizers. The convex and non-convex regularizers that are considered in our work are the  $\ell_1$ -norm, minimax-concave penalty (MCP) (Zhang, 2010), and smoothly clipped absolute deviation (SCAD) (Fan & Li, 2001). While the  $\ell_1$ -norm is convex, the other two penalties – MCP and SCAD – are not convex. The

MCP and SCAD penalties approximate the  $\ell_0$  pseudonorm better than the  $\ell_1$  norm and hence give rise to better recovery performance (Zhang, 2010). The ideal sparse recovery problem requires minimization of the  $\ell_0$  pseudonorm, but it is NP-hard and hence tractable solvers that approximate  $\ell_0$  minimization are preferred. The MCP and SCAD penalties perfectly fit the bill and hence we consider them for composite regularization. The three penalties under consideration and the corresponding proximal operators are given in Table 1.

#### 4.1. Proximal-Averaged Iterative Shrinkage Algorithm (PAISA)

The problem in Eq. (2) is optimized based on majorization-minimization (Figueiredo et al., 2007) and proximal-averaging (Zhong & Kwok, 2014). The update  $\mathbf{x}$  at  $(k+1)^{\text{th}}$  iteration is obtained by solving the following optimization problem:

$$\min_{\mathbf{x}} \frac{1}{2\rho} \|\mathbf{x} - \mathbf{r}^{(k+1)}\|_2^2 + \sum_{i=1}^p \alpha_i g_i(\mathcal{F}(\mathbf{x})), \quad (3)$$

where  $\mathbf{r}^{(k+1)} = \mathbf{x}^{(k)} - \rho \Phi^T (\Phi \mathbf{x}^{(k)} - \mathbf{y})$  and  $\rho$  is the step-size. The above problem can be rewritten as

$$\min_{\mathbf{x}} \sum_{i=1}^p \left( \frac{\alpha_i}{2\rho} \|\mathbf{x} - \mathbf{r}^{(k+1)}\|_2^2 + \alpha_i g_i(\mathcal{F}(\mathbf{x})) \right). \quad (4)$$

Zhang & Ghanem (2018) showed that a data-driven analysis transform improves the reconstruction of natural images from the compressed measurements. Based on this observation,  $\mathcal{F}$  is chosen to be a combination of two linear convolutional operators, without bias terms, separated by a rectified linear unit (ReLU) (Nair & Hinton, 2010).  $\mathcal{F}$  can be formulated in matrix form as  $\mathcal{F}(\mathbf{x}) = \mathbf{B} \max(\mathbf{A}\mathbf{x}, \mathbf{0})$ , where  $\mathbf{A}$  and  $\mathbf{B}$  correspond to the two convolutional operators, and  $\max(\cdot, \mathbf{0})$  denotes the ReLU. The convolutional operators  $\mathbf{A}$  and  $\mathbf{B}$  use  $n_f$  filters of size  $3 \times 3$  and  $3 \times 3 \times n_f$ , respectively. Zhang et al. (2014) showed that, in the context of

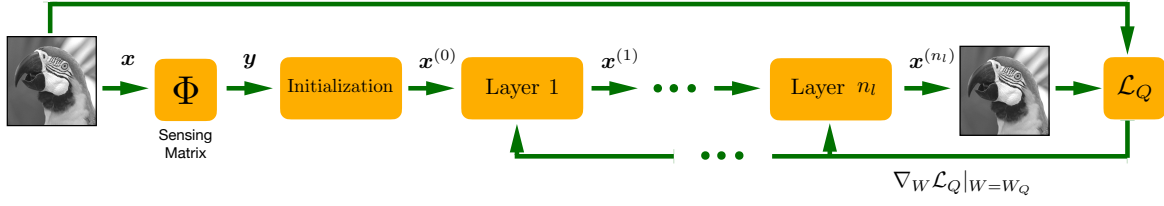


Figure 2: Illustration of the proposed Quantized Proximal Averaging Network (Q-PAN).

inverse problems in imaging, it is reasonable to assume that the elements of  $(\mathbf{x}^{(k+1)} - \mathbf{r}^{(k+1)})$  are independent normal distributed random variables with zero mean and variance  $\sigma^2$ . Let  $\mathbf{r}^{(k+1)}$  and  $\mathcal{F}(\mathbf{r}^{(k+1)})$  denote the mean values of  $\mathbf{x}$  and  $\mathcal{F}(\mathbf{x})$ , respectively. The following approximation holds (Zhang & Ghanem, 2018):

$$\|\mathcal{F}(\mathbf{x}) - \mathcal{F}(\mathbf{r}^{(k+1)})\|_2^2 \approx \beta \|\mathbf{x} - \mathbf{r}^{(k+1)}\|_2^2, \quad (5)$$

where  $\beta$  depends only on the parameters of  $\mathcal{F}$ . Incorporating the approximation in Eq. (5) into Eq. (4), we obtain (merging  $\rho$  and  $\beta$  into the parameters of the regularizers):

$$\begin{aligned} \mathbf{x}^{(k+1)} = & \arg \min_{\mathbf{x}} \sum_{i=1}^p \alpha_i \|\mathcal{F}(\mathbf{x}) - \mathcal{F}(\mathbf{r}^{(k+1)})\|_2^2 \\ & + \sum_{i=1}^p \alpha_i g_i(\mathcal{F}(\mathbf{x})). \end{aligned} \quad (6)$$

The solution to the above problem relies on proximal-averaging and is given by

$$\mathbf{x}^{(k+1)} = \tilde{\mathcal{F}} \left( \sum_{i=1}^p \alpha_i \mathcal{P}_i(\mathcal{F}(\mathbf{r}^{(k+1)})) \right), \quad (7)$$

where  $\tilde{\mathcal{F}}$  is the adjoint of  $\mathcal{F}$  such that  $\tilde{\mathcal{F}}(\mathcal{F}(\mathbf{x})) = \mathbf{x}$ . The optimization steps for minimizing the problem in Eq. (2) are listed in Algorithm 1.

## 4.2. Proximal Averaging Network (PAN)

Unfolding the iterations of PAISA (Algorithm 1) results in a feedforward neural network, which we refer to as the proximal averaging network (PAN). A single PAN layer is represented by

$$\mathbf{x}^{(k)} = \tilde{\mathcal{F}}^{(k)} \left( \sum_{i=1}^p \alpha_i \mathcal{P}_i(\mathcal{F}^{(k)}(\mathbf{r}^{(k)})) \right). \quad (8)$$

The parameters corresponding to the sparsity promoting regularizers and the analysis transform  $\{\lambda_1^{(k)}, \lambda_2^{(k)}, \lambda_3^{(k)}, a^{(k)}, \gamma^{(k)}, \mathcal{F}^{(k)}, \tilde{\mathcal{F}}^{(k)}\}$  are all learnable subject to the conditions  $\lambda_i^{(k)} > 0, \gamma^{(k)} > 1, a^{(k)} > 2$  for each layer  $k$  of the network.

## Algorithm 1 Proximal-Averaged Iterative Shrinkage Algorithm (PAISA)

---

**Input:**  $\mathbf{x}, K, \lambda_1, \lambda_2, \lambda_3, \gamma, \mathbf{a}$   
 Initialize  $\mathbf{x}_0, k = 0$ .  
**while**  $k \leq K - 1$  **do**  
 $\mathbf{x}_k = \tilde{\mathcal{F}}(\sum_{i=1}^p \alpha_i \mathcal{P}_i(\mathcal{F}(\mathbf{r}_k)))$   
 $k \leftarrow k + 1$   
**end while**

---

## 4.3. Loss Function

The loss function comprises two terms. The first term captures the mean-squared error between the ground truth  $\mathbf{x}_i$  and the reconstructed image  $\mathbf{x}_i^{(n_l)}$ , where  $n_l$  denotes the number of layers in the network. The second term seeks to enforce invertibility of the sparsifying transform  $\mathcal{F}$  across the layers. The loss function  $\mathcal{L}$  proposed in (Zhang & Ghanem, 2018) is used in our training:

$$\begin{aligned} \mathcal{L} = & \frac{1}{N} \sum_{i=1}^{n_b} \|\mathbf{x}_i^{(n_l)} - \mathbf{x}_i\|_2^2 \\ & + \gamma \frac{1}{N} \sum_{i=1}^{n_b} \sum_{k=1}^{n_l} \|\tilde{\mathcal{F}}^{(k)}(\mathcal{F}^{(k)}(\mathbf{x}_i)) - \mathbf{x}_i\|_2^2, \end{aligned} \quad (9)$$

where  $n_b$  is the number of training patches extracted from the images in the dataset,  $n$  is the size of each training patch,  $n_l$  is the number of layers of the network,  $N = n_b n$ , and  $\gamma$  determines the trade-off between the two terms under consideration.  $\gamma$  is fixed at 0.01 in our experiments.

## 4.4. PAISA<sup>+</sup> Update

The residuals (defined as the difference between the ground truth and its prediction) of natural images and videos are compressible (Sullivan et al., 2012; Wallace, 1991). The residual learning framework named ResNet (He et al., 2015) explicitly formulates the layers of the network to learn residual functions with reference to the layer inputs. Drawing inspiration from ResNet and ISTA-Net<sup>+</sup>, we propose PAISA<sup>+</sup>, whose iterations are unfolded to yield PAN<sup>+</sup>, which learns a residual function for the update  $\mathbf{x}_{k+1}$ , instead of learning it directly as done in PAN.

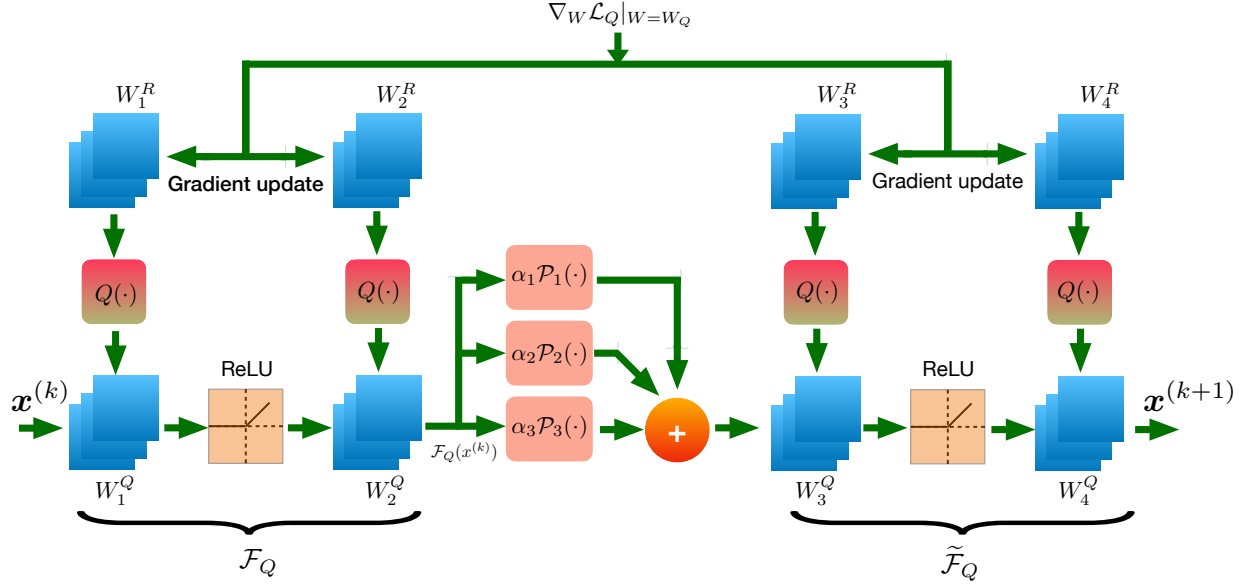


Figure 3: Structure of a layer in the Q-PAN. Quantized weights ( $\mathbf{W}_i^Q$ ) are obtained from their full precision copy ( $\mathbf{W}_i^R$ ) via quantization operator  $Q(\cdot)$ . The intermediate reconstruction  $\mathbf{x}^{(k)}$  is processed through convolution filters  $\{\mathbf{W}_i^Q\}$ , ReLU transform, proximal operators  $\{\mathcal{P}_i\}$  to give  $\mathbf{x}^{(k+1)}$ .

The update step is:  $\mathbf{x}^{(k+1)} = \mathbf{r}^{(k+1)} + \mathbf{w}^{(k+1)} + \mathbf{e}^{(k+1)}$ , where  $\mathbf{w}^{(k+1)}$  is the residual and  $\mathbf{e}^{(k+1)}$  is the error, as recommended in ISTA-Net<sup>+</sup> (Zhang & Ghanem, 2018). The residual  $\mathbf{w}^{(k+1)}$  contains the high-frequency component of  $\mathbf{x}^{(k+1)}$  missing from  $\mathbf{r}^{(k+1)}$ . It can be extracted from  $\mathbf{x}^{(k+1)}$  by an affine transformation  $\mathcal{R}$  i.e.,  $\mathbf{w}^{(k+1)} = \mathcal{R}(\mathbf{x}^{(k+1)}) = \mathcal{G}(\mathcal{D}(\mathbf{x}^{(k+1)}))$ , where  $\mathcal{D}$  has  $n_f$  filters (of size  $3 \times 3$ ) and  $\mathcal{G}$  has one filter (of size  $3 \times 3 \times n_f$ ).

To obtain a closed-form solution, we model  $\mathcal{F} = \mathcal{H} \circ \mathcal{D}$ , where  $\mathcal{H}$  is composed of two convolutional operators separated by a ReLU. Substituting  $\mathcal{F}$  in Eq. (6) by  $\mathcal{H} \circ \mathcal{D}$  gives

$$\begin{aligned} \mathbf{x}^{(k+1)} &= \arg \min_{\mathbf{x}} \frac{1}{2} \|\mathcal{H}(\mathcal{D}(\mathbf{x})) - \mathcal{H}(\mathcal{D}(\mathbf{r}^{(k+1)}))\|_2^2 \\ &\quad + \sum_{i=1}^p \alpha_i g_i(\mathcal{H}(\mathcal{D}(\mathbf{x}))). \end{aligned}$$

Following the same strategy as in PAISA, we define  $\tilde{\mathcal{H}}$ , the adjoint of  $\mathcal{H}$  to be symmetric. The PAISA<sup>+</sup> update is:

$$\begin{aligned} \mathbf{x}^{(k+1)} &= \mathbf{r}^{(k+1)} \\ &\quad + \mathcal{G} \left( \tilde{\mathcal{H}} \left( \sum_{i=1}^p \alpha_i \mathcal{P}_i(\mathcal{H}(\mathcal{D}(\mathbf{r}^{(k+1)}))) \right) \right). \end{aligned} \quad (10)$$

The iterations of PAISA<sup>+</sup> are unfolded into the layers of a neural network, henceforth referred to as PAN<sup>+</sup>. The parameters in all the layers of the model are learnable, i.e., all convolutional operators  $\mathcal{H}$ ,  $\tilde{\mathcal{H}}$ ,  $\mathcal{D}$ ,  $\mathcal{G}$  are learned in each

layer of the network, along with parameters involved in the proximal operators  $\mathcal{P}_i$ . A layer of PAN<sup>+</sup> is given by the input-output equation:

$$\begin{aligned} \mathbf{x}^{(k)} &= \mathbf{r}^{(k)} \\ &\quad + \mathcal{G}^{(k)} \left( \tilde{\mathcal{H}}^{(k)} \left( \sum_{i=1}^p \alpha_i \mathcal{P}_i(\mathcal{H}^{(k)}(\mathcal{D}^{(k)}(\mathbf{r}^{(k)}))) \right) \right). \end{aligned} \quad (11)$$

The learnable parameters in this case are  $\{\lambda_1^{(k)}, \lambda_2^{(k)}, \lambda_3^{(k)}, a^{(k)}, \gamma^{(k)}, \mathcal{H}^{(k)}, \tilde{\mathcal{H}}^{(k)}, \mathcal{D}^{(k)}, \mathcal{G}^{(k)}\}$  subject to the conditions  $\lambda_i^{(k)} > 0, \gamma^{(k)} > 1, a^{(k)} > 2$  for each layer  $k$  of the network. Also, the loss function is augmented with a new term as done in Eq. (10) to enforce the adjoint property:  $\tilde{\mathcal{H}}^{(k)} \circ \mathcal{H}^{(k)} = \mathcal{I}$ .

## 5. Quantized Deep-Unrolled Compressive Sensing Networks

We now consider the effect of quantization of weights in the network. We consider  $K$  bit quantization of the weights. We work with two versions of the filter weights – the unquantized version and the quantized version. In the forward pass of Q-PAN, the full precision weights are mapped to the quantization levels, which are determined in a minimum mean-square error sense based on the weights obtained in the backpropagation update. The gradients of the loss function are computed with respect to the quantized



**Algorithm 2** Training strategy for Q-PAN

---

**Input:**  $x, \Phi, y$   
**Output:**  $x^*$   
**for**  $y, x$  in training data **do**  
   **for**  $W_Q, \tilde{W}$  in  $\mathcal{F}_Q, \tilde{\mathcal{F}}$  **do**  
      $W_Q \leftarrow Q(W)$   
   **end for**  
   **for**  $\tilde{W}_Q, \tilde{W}$  in  $\tilde{\mathcal{F}}_Q, \tilde{\mathcal{F}}$  **do**  
      $\tilde{W}_Q \leftarrow Q(\tilde{W})$   
   **end for**  
   **for**  $k = 1 : n_b$  **do**  
      $r^{(k+1)} = x^{(k)} - \rho \Phi^T(\Phi x^{(k)} - y)$   
      $x^{(k)} = \tilde{\mathcal{F}}_Q^{(k)}\left(\sum_{i=1}^p \alpha_i \mathcal{P}_i(\mathcal{F}_Q^{(k)}(r^{(k+1)}))\right)$   
   **end for**  
   Compute  $\mathcal{L}_Q$  per Eq. (15)  
   **for**  $W, \tilde{W}$  in  $\mathcal{F}, \tilde{\mathcal{F}}$  **do**  
      $W \leftarrow W - \delta \nabla_W \mathcal{L}_Q |_{W=W_Q}$   
      $\tilde{W} \leftarrow \tilde{W} - \delta \nabla_{\tilde{W}} \mathcal{L}_Q |_{W=\tilde{W}_Q}$   
   **end for**  
**end for**

---

weights. The weight updates happen on the full-precision version. The training strategy for Q-PAN models has been captured in Algorithm 2, where  $Q(\cdot)$  denotes the quantization operator, defined in Fig. 3. The quantization scheme is learnable.  $Q(x) = v \cdot b$ , where  $b$  has integer entries and  $v$  is a scale factor. The scale factor is “learned” from the data  $x$ . Effectively, we are learning to match the dynamic range of the quantizer to that of the data.

The non-linear sparsifying transform  $\mathcal{F}$  in Eq. (2) is modeled using a convolution network. In Q-PAN, a learnable quantization scheme maps the filter weights to lower-precision weights resulting in a quantized transform  $\mathcal{F}_Q$ . The sparsifying transform ( $\mathcal{F}_Q$ ) is represented by conjunction of quantized convolution filters with ReLU. The update  $x$  at  $(k+1)^{\text{th}}$  iteration with the quantized transform is given by

$$x_{k+1} = \arg \min_x J(x), \quad (12)$$

where

$$J(x) = \sum_{i=1}^p \frac{\alpha_i}{2\rho} \|x - r^{(k+1)}\|_2^2 + \sum_{i=1}^p \alpha_i g_i(\mathcal{F}_Q(x)),$$

$\rho$  is the step-size and  $r^{(k+1)} = x^{(k)} - \rho \Phi^T(\Phi x^{(k)} - y)$ .  $\mathcal{F}_Q$  could be expressed in matrix form as  $\mathcal{F}_Q(x) = \mathbf{B}_Q \max(\mathbf{A}_Q x, \mathbf{0})$ , where  $\mathbf{A}_Q$  and  $\mathbf{B}_Q$  correspond to the convolutional operators with quantized weights. Following the procedure outlined in Section 4, the structure of a layer

in Q-PAN is modelled as follows:

$$x = \tilde{\mathcal{F}}_Q \left( \sum_{i=1}^p \alpha_i \mathcal{P}_i(\mathcal{F}_Q(r)) \right), \quad (13)$$

where the learnable parameters are  $\{\lambda_i, a, \gamma, \mathcal{F}_Q, \tilde{\mathcal{F}}_Q\}$  subject to the conditions  $\lambda_i > 0, \gamma > 1, a > 2$ . The Q-PAN architecture is depicted visually in Figure 2. Similarly, each layer of the Q-PAN<sup>+</sup> model is given by:

$$x = r + \mathcal{G}_Q(\tilde{\mathcal{H}}_Q(\sum_{i=1}^p \alpha_i \mathcal{P}_i(\mathcal{H}_Q(\mathcal{D}_Q(r))))). \quad (14)$$

The weights of Q-PAN<sup>+</sup> are also quantized to  $K$ -bits. The loss function with weight quantization in the learning framework is given by

$$\begin{aligned} \mathcal{L}_Q = & \frac{1}{N} \sum_{i=1}^{n_b} \|x_i^{n_i} - x_i\|_2^2 \\ & + \gamma \frac{1}{N} \sum_{i=1}^{n_b} \sum_{k=1}^{n_i} \|\tilde{\mathcal{F}}_Q^{(k)}(\mathcal{F}_Q^{(k)}(x_i)) - x_i\|_2^2. \end{aligned} \quad (15)$$

Once the training is completed, only the quantized version of the weights is retained for inference. The architecture of one layer of Q-PAN is depicted in Fig. 3.

## 6. Experimental Results and Discussion

We validate the performance of our networks, PAN, PAN<sup>+</sup> and their quantized counterparts, namely, Q-PAN and Q-PAN<sup>+</sup> on natural image recovery and MR image reconstruction from compressed measurements. The results corresponding to PAN<sup>+</sup> and Q-PAN<sup>+</sup> are reported here. Due to space constraints, the results corresponding to PAN and Q-PAN are reported in the Supplementary Document. For performance assessment and comparison, we use peak signal-to-noise ratio (PSNR) and structural similarity index metric (SSIM) (Zhou Wang et al., 2004).

Several CS techniques (Kulkarni et al., 2016; Li et al., 2013; Metzler et al., 2016; Mousavi et al., 2015; Zhang et al., 2017) are shown to be under-performing in comparison to ISTA-Net and ISTA-Net<sup>+</sup> (Zhang & Ghanem, 2018). Therefore we compare the proposed PAN<sup>+</sup> and Q-PAN<sup>+</sup> models with ISTA-Net<sup>+</sup> and quantized ISTA-Net<sup>+</sup> (Q-ISTA-Net<sup>+</sup>) in the context of compressed image reconstruction. ISTA-Net<sup>+</sup> uses single regularizer i.e.  $\ell_1$  penalty, where as PAN<sup>+</sup> (3R) models employs two additional regularizers (SCAD and MCP). The performance improvement of PAN<sup>+</sup> (3R) over ISTA-Net<sup>+</sup> authenticates the superiority of three regularizers over one.

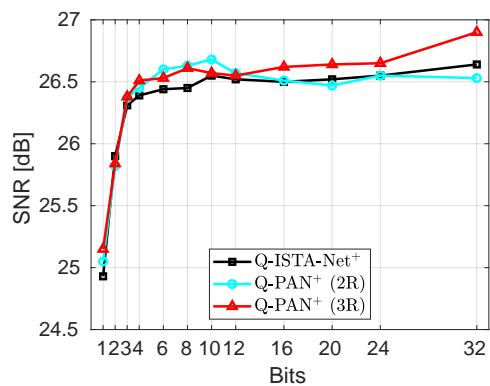
To ensure fair comparison, we use the same set of images as recommended in (Zhang & Ghanem, 2018) to train our models. The loss function, number of layers in the networks, the

Table 2: PSNR [dB] comparison between quantized and unquantized networks on *Set11* dataset between techniques from literature and Q-PAN<sup>+</sup> (3R) models.

CS RATIO	SDA	RECON NET	ISTA-NET	ISTA-NET <sup>+</sup>	PAN <sup>+</sup>	1-BIT Q-PAN <sup>+</sup>	2-BIT Q-PAN <sup>+</sup>	3-BIT Q-PAN <sup>+</sup>
1%	17.29	17.27	17.30	17.34	17.43	17.46	17.48	<b>17.49</b>
4%	20.12	20.63	21.23	21.31	<b>21.83</b>	20.95	21.20	21.47
10%	22.65	24.28	25.80	26.64	<b>26.90</b>	25.15	25.84	26.38

 Table 3: Comparison between quantized and unquantized networks over average PSNR [dB] values on BSD68 dataset for different compression ratios. The PAN<sup>+</sup> models are of 3R variant

CS RATIO	ISTA-NET <sup>+</sup>	PAN <sup>+</sup>	1-BIT Q-PAN <sup>+</sup>	3-BIT Q-PAN <sup>+</sup>
10%	25.33	<b>25.48</b>	24.69	25.27
4%	22.17	<b>22.49</b>	21.96	22.28
1%	19.17	<b>19.21</b>	19.15,	19.21


 Figure 4: Comparative performance of Quantized ISTA-Net<sup>+</sup>, Q-PAN<sup>+</sup> (2R) and Q-PAN<sup>+</sup> (3R) on Set11 dataset for CS Ratio = 10 with varying quantization bits

size and number of filters learned in the sparsifying function  $\mathcal{F}$  are maintained the same for all the networks under consideration. The compressed measurements  $\mathbf{y}$  are computed as  $\mathbf{y} = \Phi\mathbf{x}$ , where  $\Phi \in \mathbb{R}^{m \times n}$  and  $m$  varies depending on the compressive sensing (CS) ratio. The measurement matrix  $\Phi$  is obtained by orthonormalizing the rows of a random Gaussian matrix. In training our models, we set the batch size  $n_b$  to 64, and the number of layers  $n_l$  as 9. In the transform  $\mathcal{F}$ ,  $n_f = 32$  filters of size  $3 \times 3$  are learned in the first convolutional operation. The second convolutional operator learns  $n_f = 32$  filters each of size  $3 \times 3 \times 32$ .

The training data consists of 88,912 cropped image patches each of size  $33 \times 33$ . We trained the network models considering CS ratios of 1%, 4% and 10%. The training and infer-

ence is carried out on a workstation with dual Intel® Xeon® Silver 4110 processors and RTX2080Ti GPU. The models are trained for 100 epochs and take approximately 9 hours. The PAN<sup>+</sup> (2R), Q-PAN<sup>+</sup> (2R) models employ two regularizers, namely the  $\ell_1$  penalty and the MC penalty. The convex combination weights are fixed as  $\alpha_1 = \alpha_2 = \frac{1}{2}$ . The PAN<sup>+</sup> (3R), Q-PAN<sup>+</sup> (3R) models additionally use the SCAD penalty alongside  $\ell_1$  and the MCP with  $\alpha_1 = \alpha_2 = \alpha_3 = \frac{1}{3}$ .

The models are tested on the widely used Set11 (Kulkarni et al., 2016) and BSD68 (Martin et al., 2001) datasets, which contain 11 and 68 grayscale images respectively. We report the average PSNR over the test images in Table 3. To compare the effect of quantization on various models, we trained quantized versions of ISTA-Net<sup>+</sup> also. The variation of PSNR with the change in quantization bit-width is captured in Figure 4. We observe that Q-PAN<sup>+</sup> (3R) outperforms Q-ISTA-Net<sup>+</sup> consistently across different quantizations. The CS reconstructions by the proposed models are shown in Figs. 5 and 6 for visual inspection. From the zoomed-in figure (cf. Fig. 5), one can infer that the PAN<sup>+</sup> (3R) model preserves the structure of the ground truth better, in comparison to the benchmark reconstructions. From the reconstruction error images (cf. Fig. 6) from the 1-bit quantized models, one can observe that the Q-PAN<sup>+</sup> (3R) model contains fewer artefacts in its reconstruction.

## 6.1. MR image reconstruction

We evaluate the effectiveness of PAN<sup>+</sup> and Q-PAN<sup>+</sup> models on the CS MRI problem. The MR image reconstruction methods sample data in the Fourier space and adopt the CS theory to reconstruct images. During the reconstruction, the sensing matrix is obtained through a combination of under-sampling matrix  $\mathbf{P}$  and a discrete Fourier Transform matrix  $\mathbf{F}$  as in  $\Phi = \mathbf{P}\mathbf{F}$ . We use the same training and testing brain medical images as in (Zhang & Ghanem, 2018), and train models with  $n_l = 11$  layers for CS ratios of 20%, 30%, 40%, 50%. The comparison between ISTA-Net<sup>+</sup>, PAN<sup>+</sup> (3R), and 1-bit Q-PAN<sup>+</sup> (3R) techniques is summarized in Table 4. The experimental results shows that PAN<sup>+</sup> outperforms ISTA-Net<sup>+</sup> for all the compression ratios under consideration. Even when extremely quantized 1-bit representations are used, one can observe that the reconstruction performance degradation is at most 0.56 dB.

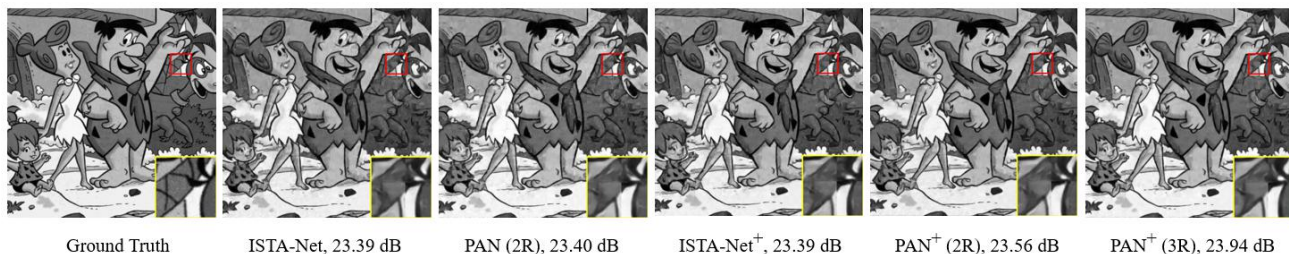

 Figure 5: Reconstruction results for *Flintstones* image based on 10% compressed measurements.

Table 4: Comparison of average PSNR [dB] on MR images between techniques from the literature and proposed models with three regularizers.

CS RATIO	ADMM-NET	ISTA-NET	ISTA-NET <sup>+</sup>	PAN <sup>+</sup>	1-BIT Q-PAN <sup>+</sup>	2-BIT Q-PAN <sup>+</sup>	3-BIT Q-PAN <sup>+</sup>
20%	37.17	38.30	38.73,	38.90	38.17	38.55	<b>39.13</b>
30%	39.84	40.52	40.89,	41.02	40.36	40.76	<b>41.32</b>
40%	41.56	42.12	42.52	42.71	42.41	42.60	<b>43.04</b>
50%	43.00	43.60	44.09	44.29	43.84	44.29	<b>44.41</b>

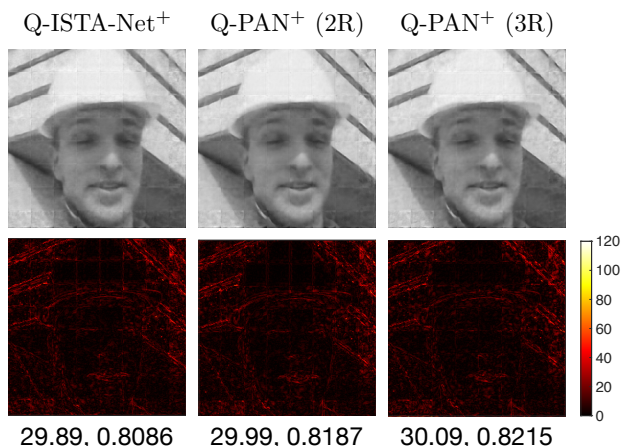
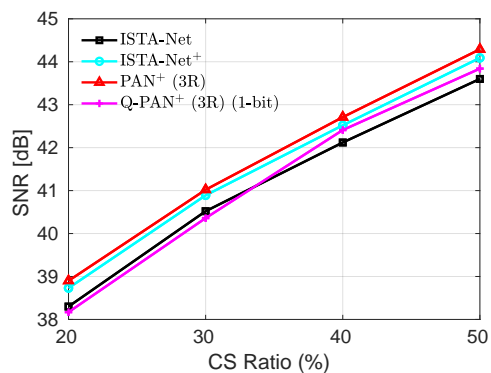


Figure 6: Foreman (Set11) image reconstruction for CS ratio 10% by the proposed 1-bit Quantized models. The bottom row visualizes the absolute difference between the ground truth and the reconstructed images. The numbers indicate the PSNR, SSIM values.

## 7. Conclusion

We proposed a multi-penalty formulation for the problem of compressed image reconstruction to learn data-driven analysis prior and developed proximal-averaged iterative shrinkage algorithm for solving it. We then unfolded the iterations to obtain a neural network architecture. Making use of the knowledge that natural images are compressible in the residual domain, the enhanced network PAN<sup>+</sup> is pro-


 Figure 7: MR Image Reconstruction: Performance comparison of Q-PAN<sup>+</sup> with the full-precision models, namely, PAN (Ours), ISTA-Net, and ISTA-Net<sup>+</sup> in terms of PSNR as a function of CS ratio. One can infer that Q-PAN<sup>+</sup> with 1-bit quantization achieves image reconstruction performance on par with that of the full-precision models.

posed. We then incorporated a novel learnable quantization strategy into the unfolded networks and showed that the performance degradation even considering the extreme case of 1-bit quantization is less than 1 dB compared with the full precision case. The results present strong evidence that unfolded proximal-averaging networks with a quantizer incorporated into the loop in the learning stage offers competitive performance compared with the full-precision case. This makes a strong case for deployment of such networks on low-precision hardware.



## References

- Beck, A. and Teboulle, M. A fast iterative shrinkage-thresholding algorithm for linear inverse problems. *SIAM Journal on Imaging Sciences*, 2(1):183–202, 2009.
- Courbariaux, M., Bengio, Y., and David, J.-P. Binaryconnect: Training deep neural networks with binary weights during propagations. In *Advances in neural information processing systems*, pp. 3123–3131, 2015. URL <https://arxiv.org/pdf/1511.00363.pdf>.
- Deng, J., Dong, W., Socher, R., Li, L.-J., Li, K., and Fei-Fei, L. ImageNet: A Large-Scale Hierarchical Image Database. In *CVPR09*, 2009.
- Donoho, D. L., Maleki, A., and Montanari, A. Message-passing algorithms for compressed sensing. in *Proceedings of the National Academy of Sciences, U.S.A.*, 106(45):18914–18919, 2009.
- Duncan, K., Komendantskaya, E., Stewart, R., and Lones, M. Relative robustness of quantized neural networks against adversarial attacks. In *2020 International Joint Conference on Neural Networks (IJCNN)*, pp. 1–8, 2020. doi: 10.1109/IJCNN48605.2020.9207596.
- Elad, M., Milanfar, P., and Rubinstein, R. Analysis versus synthesis in signal priors. *Inverse Problems*, 23(3):947, 2007.
- Fan, J. and Li, R. Variable selection via nonconcave penalized likelihood and its oracle properties. *Journal of the American Statistical Association*, 96:1348–1360, 02 2001. doi: 10.1198/016214501753382273.
- Figueiredo, M. A., Bioucas-Dias, J. M., and Nowak, R. D. Majorization-minimization algorithms for wavelet-based image restoration. *IEEE Transactions on Image Processing*, 16(12):2980–2991, 2007.
- He, K., Zhang, X., Ren, S., and Sun, J. Deep residual learning for image recognition. *CoRR*, abs/1512.03385, 2015. URL <http://arxiv.org/abs/1512.03385>.
- Hubara, I., Courbariaux, M., Soudry, D., El-Yaniv, R., and Bengio, Y. Binarized neural networks. In *Advances in Neural Information Processing Systems*, volume 29, pp. 4107–4115. Curran Associates, Inc., 2016.
- Hubara, I., Courbariaux, M., Soudry, D., El-Yaniv, R., and Bengio, Y. Quantized neural networks: Training neural networks with low precision weights and activations. *Journal of Machine Learning Research*, 18(187):1–30, 2018.
- Jacob, M., Ye, J. C., Ying, L., and Doneva, M. Computational MRI: Compressive Sensing and Beyond. *IEEE Signal Processing Magazine*, 37(1):21–23, 2020. doi: 10.1109/MSP.2019.2953993.
- Kamilov, U. S. A parallel proximal algorithm for anisotropic total variation minimization. *IEEE Transactions on Image Processing*, 26(2):539–548, 2017. doi: 10.1109/TIP.2016.2629449.
- Kim, Y., Nadar, M. S., and Bilgin, A. Compressed sensing using a gaussian scale mixtures model in wavelet domain. In *2010 IEEE International Conference on Image Processing*, pp. 3365–3368, 2010. doi: 10.1109/ICIP.2010.5652744.
- Krizhevsky, A., Nair, V., and Hinton, G. Cifar-10 (canadian institute for advanced research). URL <http://www.cs.toronto.edu/~kriz/cifar.html>.
- Kulkarni, K., Lohit, S., Turaga, P., Kerviche, R., and Ashok, A. ReconNet: Non-iterative Reconstruction of Images from Compressively Sensed Measurements. In *2016 IEEE Conference on Computer Vision and Pattern Recognition (CVPR)*, pp. 449–458, 2016. doi: 10.1109/CVPR.2016.55.
- LeCun, Y. and Cortes, C. MNIST handwritten digit database. 2010. URL <http://yann.lecun.com/exdb/mnist/>.
- Li, C., Yin, W., Jiang, H., and Zhang, Y. An efficient augmented lagrangian method with applications to total variation minimization. *Computational Optimization and Applications*, 56:507–530, 12 2013. doi: 10.1007/s10589-013-9576-1.
- Liu, Y., Zhan, Z., Cai, J. F., Guo, D., Chen, Z., and Qu, X. Projected iterative soft-thresholding algorithm for tight frames in compressed sensing magnetic resonance imaging. *IEEE Transactions on Medical Imaging*, 35(9):2130–2140, 2016.
- Liu, Z., Wu, B., Luo, W., Yang, X., Liu, W., and Cheng, K. Bi-Real Net: Enhancing the Performance of 1-bit CNNs with Improved Representational Capability and Advanced Training Algorithm. *CoRR*, abs/1808.00278, 2018.
- Martin, D., Fowlkes, C., Tal, D., and Malik, J. A database of human segmented natural images and its application to evaluating segmentation algorithms and measuring ecological statistics. In *ICCV*, volume 2, pp. 416–423 vol.2, 2001. doi: 10.1109/ICCV.2001.937655.
- Meng, X., Bachmann, R., and Khan, M. E. Training binary neural networks using the Bayesian learning rule. In *Proceedings of the 37th International Conference on Machine Learning*, volume 119 of *Proceedings of Machine Learning Research*, pp. 6852–6861. PMLR, 13–18 Jul 2020.

- Metzler, C. A., Maleki, A., and Baraniuk, R. G. From denoising to compressed sensing. *IEEE Transactions on Information Theory*, 62(9):5117–5144, 2016.
- Mousavi, A., Patel, A. B., and Baraniuk, R. G. A deep learning approach to structured signal recovery. *53rd Annual Allerton Conference on Communication, Control, and Computing*, pp. 1336–1343, 2015.
- Nair, V. and Hinton, G. Rectified Linear Units Improve Restricted Boltzmann Machines. in *Proceedings of the International Conference on Machine Learning*, 27:807–814, 06 2010.
- Quinsac, C., Basarab, A., Kouamé, D., and Grégoire, J. 3D Compressed sensing ultrasound imaging. In *2010 IEEE International Ultrasonics Symposium*, pp. 363–366, 2010. doi: 10.1109/ULTSYM.2010.5935479.
- Rastegari, M., Ordonez, V., Redmon, J., and Farhadi, A. XNOR-Net: ImageNet Classification Using Binary Convolutional Neural Networks, 2016. URL <http://arxiv.org/abs/1603.05279>. cite arxiv:1603.05279.
- Rubinstein, R., Peleg, T., and Elad, M. Analysis K-SVD: A Dictionary-Learning Algorithm for the Analysis Sparse Model. *IEEE Transactions on Signal Processing*, 61(3): 661–677, 2013. doi: 10.1109/TSP.2012.2226445.
- Stinco, P., Greco, M., Gini, F., and Manna, M. L. Compressed spectrum sensing in cognitive radar systems. In *2014 IEEE International Conference on Acoustics, Speech and Signal Processing (ICASSP)*, pp. 81–85, 2014. doi: 10.1109/ICASSP.2014.6853562.
- Sullivan, G. J., Ohm, J.-R., Han, W., and Wiegand, T. Overview of the High Efficiency Video Coding (HEVC) Standard. *IEEE Transactions on Circuits and Systems for Video Technology*, 22(12):1649–1668, 2012.
- Sungkwang Mun and Fowler, J. E. Block compressed sensing of images using directional transforms. In *2009 16th IEEE International Conference on Image Processing (ICIP)*, pp. 3021–3024, 2009. doi: 10.1109/ICIP.2009.5414429.
- Tian, Z. and Giannakis, G. B. Compressed sensing for wideband cognitive radios. In *2007 IEEE International Conference on Acoustics, Speech and Signal Processing - ICASSP '07*, volume 4, pp. IV–1357–IV–1360, 2007. doi: 10.1109/ICASSP.2007.367330.
- Wallace, G. K. The JPEG Still Picture Compression Standard. *Communications of the ACM*, 34:31–44, April 1991.
- Wan, D., Shen, F., Liu, L., Zhu, F., Huang, L., Yu, M., Shen, H. T., and Shao, L. Deep quantization generative networks. *Pattern Recognition*, 105:107338, 2020. ISSN 0031-3203. doi: <https://doi.org/10.1016/j.patcog.2020.107338>.
- Wang, P., Wang, D., Ji, Y., Xie, X., Song, H., Liu, X., Lyu, Y., and Xie, Y. QGAN: quantized generative adversarial networks. *CoRR*, abs/1901.08263, 2019. URL <http://arxiv.org/abs/1901.08263>.
- Willett, R. M., Marcia, R. F., and Nichols, J. Compressed sensing for practical optical imaging systems: A tutorial. In *IEEE Photonics Conference 2012*, pp. 586–586, 2012. doi: 10.1109/IPCon.2012.6358756.
- Zhang, C.-H. Nearly unbiased variable selection under minimax concave penalty. *The Annals of Statistics*, 38(2): 894–942, 2010.
- Zhang, D., Yang, J., Ye, D., and Hua, G. Lq-nets: Learned quantization for highly accurate and compact deep neural networks. *CoRR*, abs/1807.10029, 2018.
- Zhang, J. and Ghanem, B. ISTA-Net: Interpretable optimization-inspired deep network for image compressive sensing. in *Proceedings of International Conference on Computer Vision and Pattern Recognition*, pp. 1828–1837, 2018.
- Zhang, J., Zhao, C., Zhao, D., and Gao, W. Image compressive sensing recovery using adaptively learned sparsifying basis via  $\ell_0$  minimization. *Signal Processing*, 103: 114–126, 10 2014. doi: 10.1016/j.sigpro.2013.09.025.
- Zhang, J., Zhao, D., and Gao, W. Group-based sparse representation for image restoration. *IEEE Transactions on Image Processing*, 23(8):3336–3351, 2014.
- Zhang, K., Zuo, W., Gu, S., and Zhang, L. Learning deep CNN denoiser prior for image restoration. In *in Proceedings of International Conference on Computer Vision and Pattern Recognition*, pp. 2808–2817, 2017. doi: 10.1109/CVPR.2017.300.
- Zhong, L. W. and Kwok, J. T. Gradient descent with proximal average for nonconvex and composite regularization. *Twenty Eighth AAAI Conference on Artificial Intelligence*, 3:2206–2212, 01 2014.
- Zhou Wang, Bovik, A. C., Sheikh, H. R., and Simoncelli, E. P. Image quality assessment: from error visibility to structural similarity. *IEEE Transactions on Image Processing*, 13(4):600–612, 2004. doi: 10.1109/TIP.2003.819861.

Zhu, B., Al-Ars, Z., and Hofstee, H. P. Nasb: Neural architecture search for binary convolutional neural networks. In *2020 International Joint Conference on Neural Networks (IJCNN)*, pp. 1–8, 2020. doi: 10.1109/IJCNN48605.2020.9207674.